PAPER

Cost-effective hole transporting material for stable and efficient perovskite solar cells with fill factors up to 82%†

Lei Guan,‡[ab] Xinxing Yin,‡[c] Dewei Zhao, [ID] ‡[b] Changlei Wang,[b] Qiaoshi An,[d] Jiangsheng Yu,[c] Niraj Shrestha,[b] Corey R. Grice,[b] Rasha A. Awni,[b] Yue Yu, [ID] [b] Zhaoning Song, [ID] [b] Jie Zhou,[c] Weiwei Meng,[b] Fujun Zhang, [ID] [d] Randy J. Ellingson,[b] Jianbo Wang,*[ae] Weihua Tang*[c] and Yanfa Yan [ID] *[b]

A new small molecule-based hole selective material (HSM), 4,4′,4″-(7,7′,7″-(5,5,10,10,15,15-hexahexyl-10,15-dihydro-5*H*-diindeno[1,2-*a*:1′,2′-*c*]fluorene-2,7,12-triyl)tris(2,3-dihydrothieno[3,4-*b*][1,4]dioxine-7,5-diyl))tris(*N*,*N*-bis(4-methoxyphenyl)aniline) (TRUX-E-T), has been developed by a facile synthesis with reduced cost. The highest occupied molecular orbital energy level and lowest unoccupied molecular orbital energy level of TRUX-E-T are −5.10 and −2.50 eV, respectively, making it a suitable HSM for lead iodide perovskite solar cells. TRUX-E-T can be smoothly deposited onto perovskite layers, enabling efficient perovskite solar cells with thin TRUX-E-T layers (∼50 nm), which helps cut the unit cost of the HSL used in PVSCs to approximately one-fortieth (1/40) of 2,2′,7,7′-tetrakis (*N*,*N*-di-*p*-methoxyphenylamino)-9,9′-spirobifluorene (spiro-OMeTAD). Additionally, TRUX-E-T exhibits hole mobilities as high as 2.47×10^{-4} cm^2 V^{-1} s^{-1}, better than spiro-OMeTAD. As a result, our perovskite solar cells using TRUX-E-T have shown high fill factors up to 82%. The champion cell achieved a maximum power conversion efficiency of 18.35% (16.44%) when measured under reverse (forward) voltage scan under AM1.5 G 100 mW cm^{-2} illumination. Our un-encapsulated cells exhibited good stability in ambient air, maintaining 96.4% of their initial efficiency of 18.35% after 20 days of storage.

1. Introduction

Perovskite solar cells (PVSCs) have attracted enormous attention in recent years due to their high optical absorption coefficients and very long carrier lifetimes.[1–6] The power conversion efficiency (PCE) has increased from 3.8% to over 22% in the past few years.[7–16] PVSCs are typically fabricated by sandwiching a perovskite absorber layer with an electron selective layer (ESL) and a hole selective layer (HSL). The ESL and HSL separate and extract photogenerated electrons and holes in the perovskite absorber, respectively. Therefore, the PCE of a PVSC relies significantly on the optoelectronic properties of ESL and HSL materials, such as the energy levels of band edges, bandgaps, and carrier mobility. Inappropriate ESLs and HSLs can adversely affect the open-circuit voltages (V_{oc}s) and fill factors (FFs) of PVSCs.[17,18] So far, PVSCs with record PCEs typically use TiO$_2$ ESLs and 2,2′,7,7′-tetrakis (*N*,*N*-di-*p*-methoxyphenylamino)-9,9′-spirobifluorene (spiro-OMeTAD) HSLs.[7,19] The main drawbacks of using spiro-OMeTAD HSLs in PVSCs include: (1) high cost of synthesizing pure spiro-OMeTAD; (2) poor charge transport mobility; (3) requirements for p-type dopants such as cobalt complexes which may result in chemical degradation;[20] (4) low thermal stability and crystallization at temperatures as low as 60 °C. These drawbacks limit the large-scale commercialization of PVSCs using spiro-OMeTAD HSLs. Compared with polymer semiconductors, organic small-molecule HSLs have some unique advantages, such as easy modification and purification, low-cost solution processing at low temperature, well-defined chemical structures, and molecular weights with negligible batch-to-batch variation.[21–24] For example, triazatruxene is one of such organic small-molecule HSL materials and has been successfully used as a HTL for PVSCs.[25,26] However, the synthesis of triazatruxene involves

*a*School of Physics and Technology, Center for Electron Microscopy, MOE Key Laboratory of Artificial Micro- and Nano-structures, Institute for Advanced Studies, Wuhan University, Wuhan 430072, China. E-mail: wang@whu.edu.cn

*b*Department of Physics and Astronomy, Wright Center for Photovoltaics Innovation and Commercialization, The University of Toledo, Toledo, OH 43606, USA. E-mail: yanfa.yan@utoledo.edu

*c*Key Laboratory of Soft Chemistry and Functional Materials, Nanjing University of Science and Technology, Nanjing 210094, China. E-mail: whtang@njust.edu.cn

*d*Key Laboratory of Luminescence and Optical Information, Beijing Jiaotong University, Beijing 100044, China

*e*Science and Technology of High Strength Structural Materials Laboratory, Central South University, Changsha 410083, China

† Electronic supplementary information (ESI) available. See DOI: 10.1039/c7ta08053k

‡ These authors contributed equally to this work.

a harsh phosphorus oxychloride reagent that greatly hinders its large-scale application.[25,26]

Aiming to obtain an ideal HSL with low cost, high thermal stability and high hole transport without using a Co dopant, we have designed a new HSL, 4,4′,4″-(7,7′,7″-(5,5,10,10,15,15-hexa-hexyl-10,15-dihydro-5*H*-diindeno[1,2-*a*:1′,2′-*c*]fluorene-2,7,12-triyl)-tris(2,3-dihydrothieno[3,4-*b*][1,4]dioxine-7,5-diyl))tris(*N*,*N*-bis(4-methoxyphenyl)aniline) (TRUX-E-T), with a planar molecular geometry containing truxene as the core, with 3,4-ethyl-enedioxythiophene (EDOT) as a π-linker, and methoxy-substituted triphenylamine (TPA) as arms. Unlike the orthogonal spiro core, truxene has a planar and fused molecular structure, which enables the HSL to show strong π–π stacking through intermolecular interactions, thereby leading to enhanced hole mobility. The fully conjugated truxene core also provides great potential for improved thermal and optical stability. Moreover, it offers good chemical versatility to tune the solubility, 3D configuration and optoelectronic properties.[27,28] Compared to triazatruxene, truxene can be synthesized by facile methods and it consists of six hydrophobic hexyl chains which should work better for both preventing the perovskite surface from moisture and suppressing crystal growth of HSL to obtain better films.[27,29] As proven in previous reports, the incorporation of EDOT unit can enhance charge transport and improve device performance without sacrificing stability.[30,31] TPA has a 3D π-conjugated molecular configuration, which can restrict aggregation and promote exciton separation. The propeller-like structure of TPA is also beneficial for forming uniform and smooth thin films with a stable amorphous morphology and homogeneous features.[32] A combination of an EDOT bridge with TPA arms can endow TRUX-E-T with suitable energy levels and efficient hole-transporting properties.[18,25,26,33–35]

With the aforementioned considerations, we herein report on the synthesis and characterization of TRUX-E-T and its application as a HSL in efficient PVSCs. We show that high-quality TRUX-E-T can be synthesized by a facile route, ensuring a low cost. Characterizations reveal that the highest occupied molecular orbital (HOMO) and lowest unoccupied molecular orbital (LOMO) energy levels of TRUX-E-T are at −5.10 and −2.50 eV, respectively, which are suitable as HSLs for effective charge transfer in PVSCs. TRUX-E-T exhibits hole mobilities as high as 2.47×10^{-4} cm^2 V^{-1} s^{-1} as well as efficient charge transfer at the perovskite/TRUX-E-T interface. As a result, our PVSCs using TRUX-E-T have shown high fill factors (FFs) up to 82%. Additionally, TRUX-E-T can be smoothly deposited on perovskite layers, enabling PVSCs to use thin TRUX-E-T layers. Our best-performing PVSCs use only ∼50 nm-thick TRUX-E-T HSLs, which helps to reduce the unit cost of the HSL used in PVSCs to approximately one-fortieth (1/40) of that for devices made using spiro-OMeTAD. The champion cell achieved a maximum PCE of 18.35% (16.44%) when measured under reverse (forward) voltage scan under AM1.5 G 100 mW cm^{-2} illumination. Our un-encapsulated cell exhibited good stability in ambient air, maintaining 96.4% of its initial efficiency of 18.35% after 20 days of storage. It is worth noting that TRUX-E-T HSLs do not require Co complex doping, eliminating a significant route for possible degradation.

2. Experimental section

2.1. Material synthesis

TRUX-E-T. A solution of the compound 2,7,12-tribromo-5,5,10,10,15,15-hexahexyl-10,15-dihydro-5*H*-diindeno[1,2-*a*:1′,2′-*c*]fluorene (450.0 mg, 0.42 mmol) and 4-methoxy-*N*-(4-methoxyphenyl)-*N*-(4-(7-(tributylstannyl)-2,3-dihydrothieno[3,4-*b*][1,4]dioxin-5-yl)phenyl)aniline (1.1 g, 1.49 mmol) in dry toluene (40 mL) was degassed twice with N$_2$, and then Pd(PPh$_3$)$_4$ (71.9 mg, 0.062 mmol) was added. After stirring at 110 °C for 48 h under N$_2$, the mixture was cooled to room temperature. After the removal of toluene, the crude product was purified by column chromatography on silica gel (petroleum ether/ethyl acetate, 7 : 1, v/v) and recrystallized from methanol to afford TRUX-E-T (610.0 mg, 67.5%) as a light-yellow solid. ^{1}H NMR (500 MHz, CDCl$_3$, δ): 8.34 (d, *J* = 8.5 Hz, 3H), 7.85 (d, *J* = 8.1 Hz, 3H), 7.76 (s, 3H), 7.66–7.58 (m, 6H), 7.09 (d, *J* = 8.4 Hz, 12H), 6.96 (d, *J* = 8.0 Hz, 6H), 6.89–6.79 (m, 12H), 4.50–4.34 (m, 12H), 3.81 (s, 18H), 2.93 (m, 6H), 2.18–2.06 (m, 6H), 1.03–0.78 (m, 36H), 0.68–0.50 (m, 30H). ^{13}C NMR (125 MHz, CDCl$_3$, δ): 156.25, 154.56, 147.68, 141.25, 139.16, 139.06, 138.12, 127.21, 126.88, 125.11, 124.26, 121.18, 119.65, 115.09, 65.14, 65.00, 56.10, 55.90, 37.52, 31.95, 29.98, 24.43, 22.73, 22.67, 14.42, 14.32. MALDI-TOF MS: *m/z* = 2177.0612 [M + H]$^+$, calcd for C$_{141}$H$_{153}$N$_3$O$_{12}$S$_3$: 2176.0616.

2.2. Solution preparation

Perovskite precursor. The MA$_{0.7}$FA$_{0.3}$PbI$_3$ perovskite precursor was prepared using a mixture of methylammonium iodide (MAI, Dyesol), formamidinium iodide (FAI, Dyesol), lead iodide (PbI$_2$, Alfa Aesar, 99.9985%) and lead thiocyanate (Pb(SCN)$_2$, Sigma-Aldrich, 99.5%) in dimethyl sulfoxide (DMSO, Sigma-Aldrich) and *N*,*N*-dimethylformamide (DMF, Sigma-Aldrich). The details about the precursor preparation can be found in our previous papers.[34,36–38] The precursor solution was stirred on a hotplate at 60 °C for several hours. The resulting precursor was purified using a 0.45 µm filter before spin-coating.

C$_{60}$-SAM. The C$_{60}$-self-assembly (SAM) (1-Materials) was used as purchased. C$_{60}$-SAM has a concentration of 4 mg mL^{-1} in chlorobenzene (Sigma-Aldrich, 99.8%).

Spiro-OMeTAD. 2,2′,7,7′-Tetrakis(*N*,*N*′-di-*p*-methoxyphenyl-amino)-9,9′-spirobifluorene (spiro-OMeTAD) was used to fabricate the reference HSLs and deposited on the perovskite film at 2000 rpm for 60 s. The spiro-OMeTAD was co-doped using Co(ii)-bis-(trifluoromethanesulfonyl)imide (TFSI) and Li-TFSI. The spiro-OMeTAD solution was prepared by dissolving 72.3 mg spiro-OMeTAD (Shenzhen Feiming Science and Technology Co., Ltd.) in 1 mL chlorobenzene (CB) with 28 µL 4-*tert*-butylpyridine (*t*BP) (Sigma-Aldrich), 18 µL Li-TFSI (Sigma-Aldrich) (520 mg mL^{-1} in acetonitrile) and 18 µL Co(ii)-TFSI salt (FK102, Dyesol) (300 mg mL^{-1} in acetonitrile).

TRUX-E-T. A solution of TRUX-E-T/chlorobenzene (20 mg mL^{-1}) with an additive of 15 μL Li-TFSI (170 mg mL^{-1} in acetonitrile) and 8 μL tBP.

2.3. Device fabrication

The Fluorine-doped Tin Oxide (FTO) glass substrates were cleaned by ultra-sonication in diluted Micro-90 detergent, deionized water, acetone, and 2-propanol for 15 min, respectively. SnO$_2$ ETLs were deposited on FTO using a plasma-enhanced atomic layer deposition (PEALD) method[34,37–42] and then annealed on a hotplate at 100 °C for 1 hour in ambient air (approximately 25 °C and 55% relative humidity). The substrates were then transferred into a nitrogen filled glovebox. The C$_{60}$-SAM solution was spin-coated onto the SnO$_2$ layer at 3000 rpm for 1 min. The perovskite layer was deposited by dripping diethyl ether via an anti-solvent technique. The perovskite film was annealed at 100 °C for 5 min. Spiro-OMeTAD was deposited on the perovskite film at 2000 rpm for 60 s. The TRUX-E-T was spin-coated on the perovskite film at 3500 rpm for 45 s, leading to an approximately 50 nm-thick layer. A layer of 50 nm gold was finally deposited on the top of the HSLs using thermal evaporation. The active area of the device was 0.08 cm^2 as defined by a shadow mask during the Au evaporation. For hole-only devices, a 30 nm PEDOT:PSS layer was coated on an ITO substrate, followed by the deposition of a TRUX-E-T or a spiro-OMeTAD layer and then 8 nm MoO$_3$, and 75 nm Ag layers. MoO$_3$ and Ag were thermally evaporated to complete the device fabrication.

2.4. Film and device characterization

Cross-sectional scanning electron microscopy (SEM) image of the completed devices was taken with a Hitachi S-4800. Tapping-mode atomic force microscopy (AFM) images were taken with a Veeco Nanoscope V instrument. Layer thicknesses were determined using a Dektak surface profiler and cross-sectional SEM images. Samples were illuminated through the gla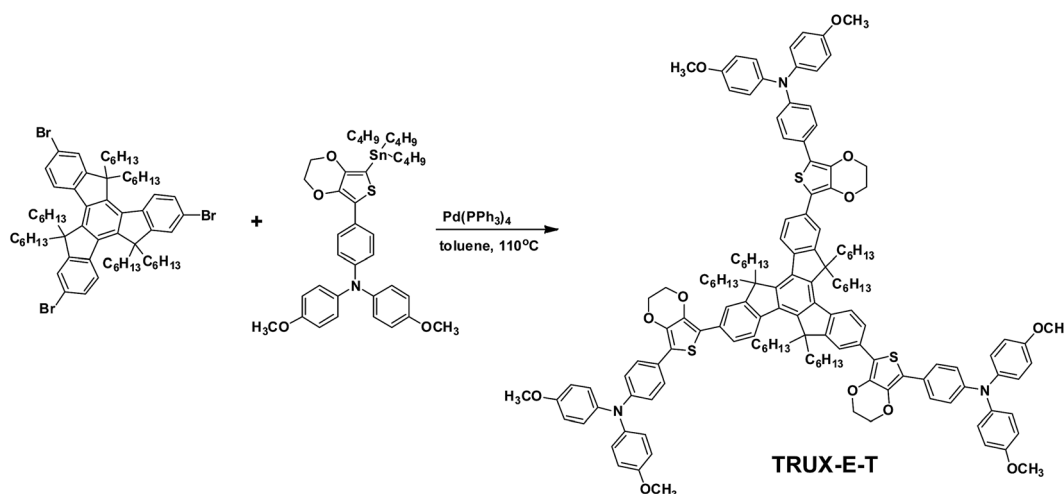ss side for photoluminescence (PL) measurements. A 532 nm cw laser at 38 mW cm^{-2} was used as a source of excitation for steady-state PL while a 532 nm pulsed laser (pulse width ~5 ps) at ~10^9 photons pulse^{-1} cm^{-2} was used as a source of excitation for TRPL measurement. PL decay curves were fitted by iterative re-convolution with the measured system response function. Mean photogenerated carrier lifetimes for the bi-exponential fit were calculated by the weighted average method.[38]

J–V curves were recorded in air under 100 mW cm^{-2} AM1.5 G solar irradiation (PV Measurements Inc.) with a Keithley 2400 Source Meter. The light intensity for J–V measurements was calibrated by using a standard Si solar cell and our perovskite solar cells certified by Newport.[16] External quantum efficiency (EQE) spectra were measured on a QE system (PV Measurements Inc., model IVQE8-C QE system without bias voltage) using 100 Hz chopped monochromatic light. The steady-state efficiencies were obtained by tracking the maximum output power point. The J–V curves for light intensity dependence were taken using neutral density filters between 1 and 100 mW cm^{-2}. The un-encapsulated cells for the stability test were stored in ambient air (45% humidity and room temperature). All characterizations and measurements were performed in ambient air.

3. Results and discussion

3.1. TRUX-E-T synthesis and characterization

The synthesis of TRUX-E-T is displayed in Scheme 1. A one-step Stille coupling of 2,7,12-tribromo-5,5,10,10,15,15-hexahexyl-10,15-dihydro-5H-diindeno[1,2-a:1′,2′-c]fluorene and 4-methoxy-N-(4-methoxyphenyl)-N-(4-(7-(tributylstannyl)-2,3-dihydrothieno[3,4-b][1,4]dioxin-5-yl)phenyl)aniline readily afforded TRUX-E-T with a yield of 67.5%. The tribromotruxene **3** was prepared via a three-step procedure, i.e., cyclization of truxene using 1-indanone, alkylation and bromination. The tin reagent was prepared according to the literature.[43] The synthetic pathways and experimental details are available in the ESI.† TRUX-E-T was acquired as a light-yellow solid after silica-gel column chromatography and recrystallization from methanol. During

Scheme 1 Synthetic route of TRUX-E-T.

This journal is © The Royal Society of Chemistry 2017

J. Mater. Chem. A, 2017, **5**, 23319–23327 | **23321**

the purification of TRUX-E-T, no expensive sublimation step is involved, which is necessary for spiro-OMeTAD instead.[44] The structure of TRUX-E-T is confirmed by ^{1}H and ^{13}C NMR spectra and MALDI-TOF mass spectrometry (Fig. S1–S6†).

Fig. S7† shows the thermogravimetric analysis (TGA) of TRUX-E-T, which exhibits a decomposition temperature (5% weight loss) of 421 °C in a nitrogen atmosphere. This result indicates the excellent inherent thermal stability of TRUX-E-T, which would benefit the long-term stability of PVSCs with TRUX-E-T HSLs. Differential scanning calorimetry (DSC) shown in Fig. S8† exhibits a clear glass transition at around 202 °C, indicating the amorphous nature of the as-synthesized TRUX-E-T.

The normalized absorption and photoluminescence (PL) spectra of a TRUX-E-T film are shown in Fig. 1a. TRUX-E-T shows absorption of photons with an edge of 477 nm and a maximum peak located at 415 nm. The shoulder in the UV region can be attributed to $\pi-\pi^*$ transition.[26] The optical bandgap (E_g^{opt}) of TRUX-E-T is estimated at 2.60 eV. The PL spectrum shows that TRUX-E-T has a main emission wavelength centred at 502 nm.

To check the energy levels of TRUX-E-T, electrochemical cyclic voltammetry (CV) was employed to evaluate its electrochemical properties. Ferrocene/ferrocenium was used as a reference with a potential of 0.55 V *vs.* the Ag/AgCl electrode. As shown in Fig. 1b, a clear oxidation peak was observed. From the onset potential for oxidation (E_{ox}), the HOMO energy level was determined to be −5.10 eV for TRUX-E-T, which is favourable for hole transfer. The corresponding LUMO energy level was estimated to be −2.50 eV according to the measured E_g^{opt}.

The electronic structure and geometry of TRUX-E-T were also investigated with density functional theory (DFT) calculation using the Gaussian program at the B3LYP/6-31G (d,p) level, as shown in Fig. 1c and d. The dihedral angles between three arms and the central truxene core are 17°, 21°, and 22°, respectively. The relatively planar molecular configuration can facilitate intermolecular interaction, and thus enhance charge transport. As shown in Fig. 1e, the calculated hole reorganization energy (λ_{hole}) of TRUX-E-T (87 meV) is much smaller than that of spiro-OMeTAD (148 meV), indicating better hole-transporting properties. We compared the hole mobility of TRUX-E-T and spiro-
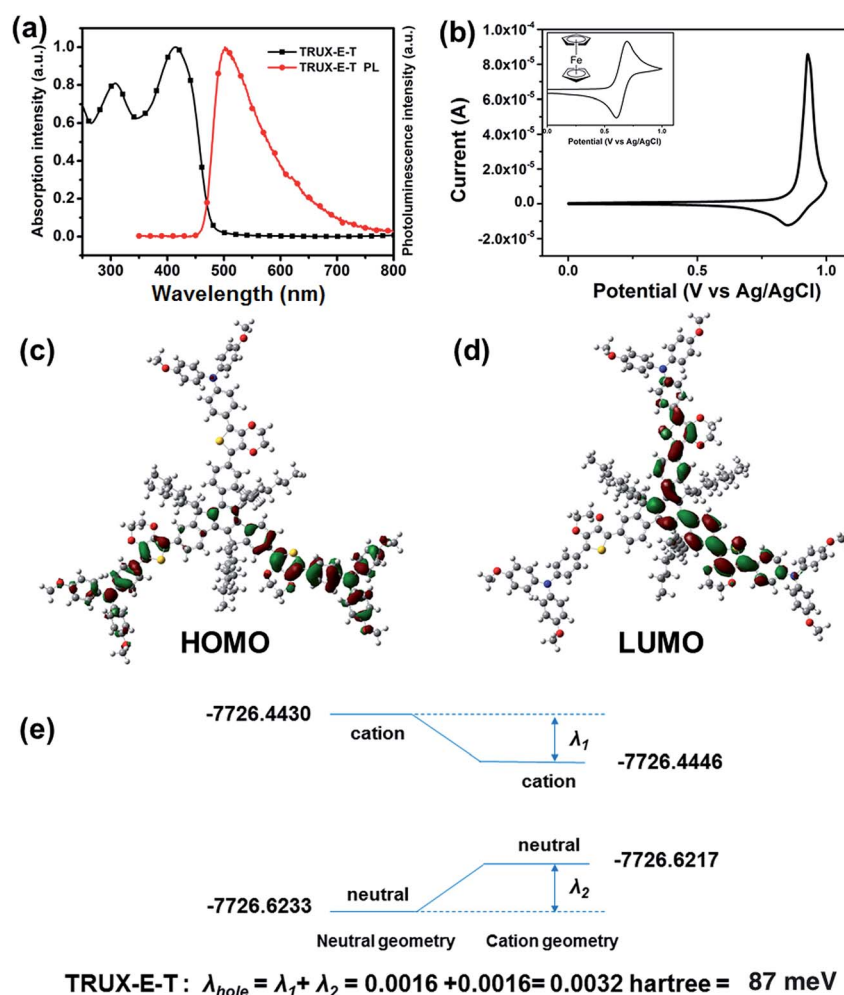

Fig. 1 (a) Absorption and PL spectra of a TRUX-E-T film. (b) Cyclic voltammetry (CV) of TRUX-E-T. The inset shows the CV plot for ferrocene/ferrocenium as a reference. The DFT-calculated electronic structure of TRUX-E-T, showing the electronic energy levels of the (c) HOMO and (d) LUMO. (e) Calculation of the hole reorganization energy for TRUX-E-T.
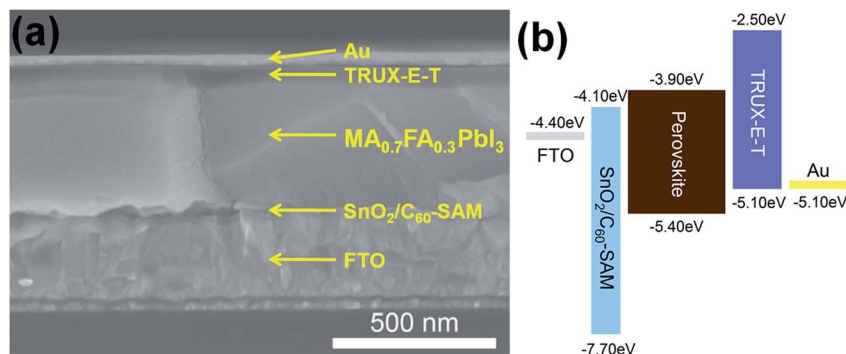
Fig. 2 (a) Cross-sectional SEM image of our regular PVSC with a TRUX-E-T HSL. (b) Energy band diagram of our regular PVSC with TRUX-E-T as the HSL.

OMeTAD by making hole-only devices with a structure of ITO/poly(3,4-ethylenedioxythiophene):polystyrene sulfonate (PEDOT:PSS)/TRUX-E-T or spiro-OMeTAD/MoO$_3$/Ag. The calculation was done by using a space charge-limited current (SCLC) model. The hole mobilities are estimated to be 1.41×10^{-4} cm^2 V^{-1} s^{-1} and 2.47×10^{-4} cm^2 V^{-1} s^{-1} for spiro-OMeTAD and TRUX-E-T, respectively, as shown in Fig. S9 (ESI†). A higher hole mobility indicates a better hole transport, benefiting the improvement in the charge transport balance within PVSCs. Our calculation and experimental characterization thus reveal that TRUX-E-T is suitable as a HSL material for PVSC fabrication.

3.2. PVSC fabrication and characterization

Fig. 2a shows a cross-sectional SEM image of our PVSC using TRUX-E-T as the HSL. The perovskite absorber is MA$_{0.7}$FA$_{0.3}$PbI$_3$ and the PVSC has the regular n–i–p configuration of FTO/SnO$_2$/C$_{60}$-SAM/perovskite/TRUX-E-T/Au. The SnO$_2$ layer was prepared by plasma-enhanced atomic-layer deposition (PEALD) and has a thickness of about 20 nm.[34,37,38,40,42] The perovskite layer was grown by a one-step deposition method and has a thickness of about 450 nm. We find that TRUX-E-T can be smoothly deposited onto the perovskite absorber layer by solution processing, as evidenced by the AFM images shown in Fig. S10.† The root mean square (RMS) roughness of the perovskite layer is

10.9 nm, which is reduced to 2.9 nm after the deposition of 50 nm TRUX-E-T. Fig. 2b shows the energy level diagram of our device using the TRUX-E-T HSL, presenting selective transfer of photogenerated electrons and holes, i.e., electrons are reflected by TRUX-E-T and transfer through SnO$_2$ and holes are reflected by SnO$_2$ and transfer through TRUX-E-T, which is suitable for PVSCs.

To evaluate the effectiveness of hole transfer at the perovskite/TRUX-E-T interface, we performed steady-state photoluminescence (PL) and time-resolved PL (TRPL) measurements on perovskite films deposited on bare glass substrates and coated with poly(methyl methacrylate) (PMMA) for protection and TRUX-E-T. As shown in Fig. 3a, the PL emission of the perovskite film with TRUX-E-T coated shows a significant quenching as compared to that of the perovskite film with PMMA coated, indicating an effective charge transfer at the perovskite/TRUX-E-T interface. The results are consistent with the TRPL decays measured from these samples (Fig. 3b). The deposition of a TRUX-E-T layer on the perovskite shortens the mean carrier lifetime for the perovskite from 650 ns to 23 ns, confirming a fast charge transfer at the perovskite/TRUX-E-T interface.

Fig. 4a shows the current density–voltage (J–V) curves of the best-performing PVSC using a 50 nm TRUX-E-T HSL measured under reverse and forward voltage scans. Our champion cell achieves a PCE of 18.36 (16.44)% with a V_{oc} of 1.08 (1.04) V, a J_{sc}
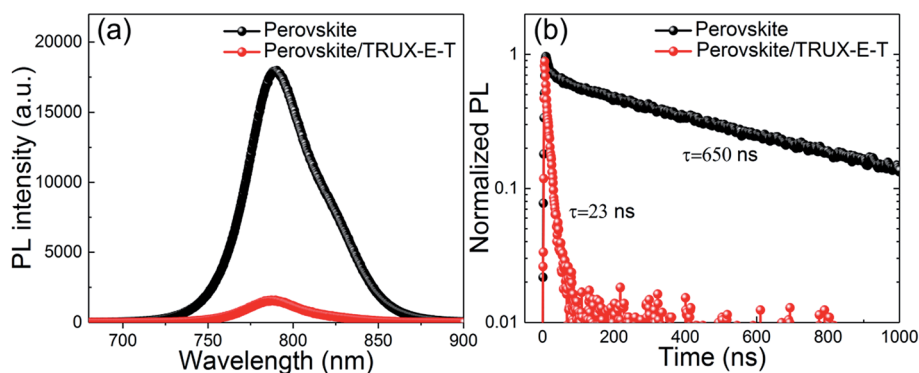

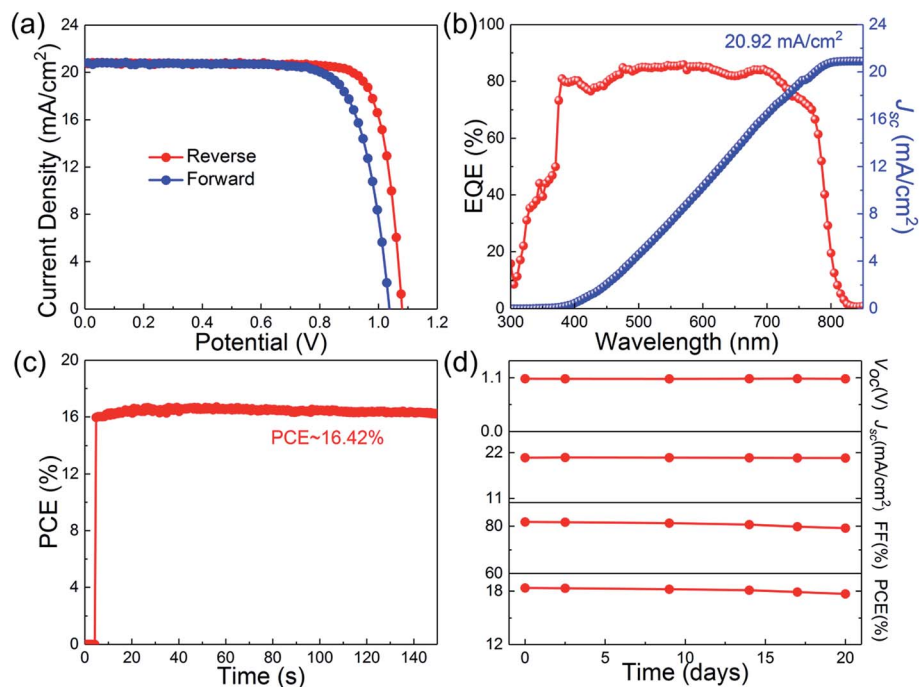Fig. 3 (a) PL spectra and (b) TRPL decays of the perovskite film and perovskite/TRUX-E-T.

This journal is © The Royal Society of Chemistry 2017

J. Mater. Chem. A, 2017, 5, 23319–23327 | 23323

Fig. 4 (a) J–V curves of our best-performing PVSC with a TRUX-E-T HSL measured under AM 1.5 G illumination at reverse and forward voltage scans. (b) EQE spectrum and integrated J_{sc} of the best-performing PVSC based on the TRUX-E-T HSL. (c) Maximum power point tracking of PCE and (d) photovoltaic parameters *versus* time of the PVSC with the TRUX-E-T HSL.

of 20.8 (20.8) mA cm^{-2}, and a FF of 81.8 (76.2)% when measured under reverse (forward) voltage scan. This performance is slightly lower than that of the PVSC with spiro-OMeTAD HSLs (PCE of 19.13 (18.12)% with a V_{oc} of 1.10 (1.09) V, a J_{sc} of 21.9 (21.9) mA cm^{-2}, and a FF of 78.7 (76.4)% under reverse (forward) voltage scan), as shown in Fig. S11.† Since the J–V
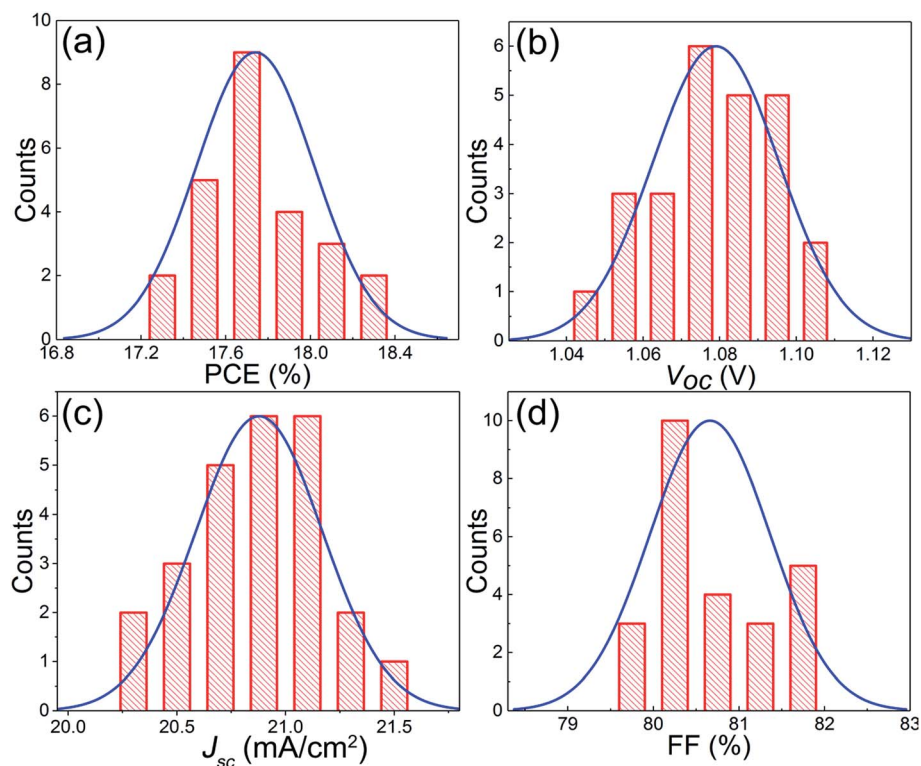

Fig. 5 Histograms of (a) PCEs, (b) V_{oc}s, (c) J_{sc}s and (d) FFs measured for 25 cells with TRUX-E-T-based PVSCs.

23324 | J. Mater. Chem. A, 2017, 5, 23319–23327

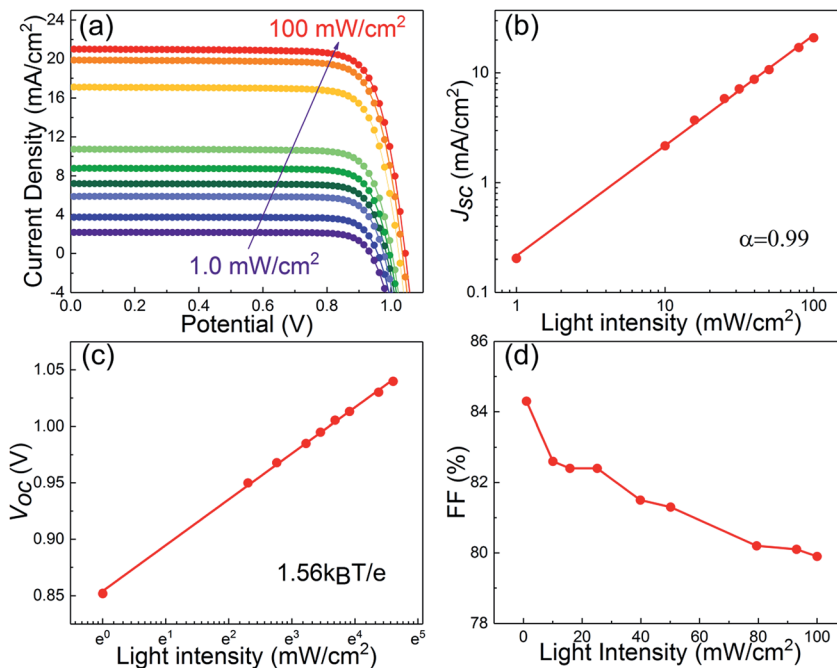This journal is © The Royal Society of Chemistry 2017

Fig. 6 (a) $J–V$ curves of a PVSC with TRUX-E-T HSLs under different light intensities ranging from 1 to 100 mW cm^{-2}. Light intensity dependence: (b) J_{sc} versus light intensity; (c) V_{oc} versus light intensity; (d) FF versus light intensity.

hysteresis was observed in both PVSCs with TRUX-E-T and spiro-OMeTAD HSLs, it might be attributed to the ESL/perovskite interface[37,40] or the perovskite film itself such as ion migration,[45] and/or trap states.[46] The EQE spectrum of this cell is shown in Fig. 4b. The integrated J_{sc} of over a 100 mW cm^{-2} AM1.5 G solar spectrum is 20.92 mA cm^{-2}, which is in good agreement with the J_{sc} obtained from the $J–V$ curves. The stabilized PCE measured by the tracking maximum power point is 16.42% (Fig. 4c). As mentioned above, TRUX-E-T has a good thermal stability, which can help to improve the stability of PVSCs. Therefore, we measured the dependence of each photovoltaic parameter of un-encapsulated PVSCs with TRUX-E-T HSLs stored in the dark and glovebox on the storage time. As shown in Fig. 4d, the cell exhibited a good stability for 20 days, maintaining 96.4% of its initial efficiency of 18.35% when measured under reverse voltage scan and under ambient conditions. The main degradation originates from FFs dropping from 81.8% to 79.2%, which is likely attributed to the contact damage of our measured cell with isolated pixels. In other words, the results suggest an encouraging alternative HSL for stable PVSCs.

To evaluate the performance reproducibility of PVSCs using the TRUX-E-T HSLs, we fabricated and measured 25 PVSCs. The histograms of the PCE, V_{oc}, J_{sc}, and FF measured under reverse voltage scan are shown in Fig. 5a, b, c, and d, respectively. The average PCE, V_{oc}, J_{sc}, and FF for these 25 cells are 17.74 ± 0.62%, 1.08 ± 0.03 V, 20.88 ± 0.65 mA cm^{-2}, and 80.7 ± 1.2%, respectively, revealing a good reproducibility.

To understand the charge extraction and recombination mechanism in the PVSCs with TRUX-E-T HSLs, the $J–V$ characteristics were measured under light intensities varying from 1 to 100 mW cm^{-2}, as shown in Fig. 6a. Fig. 6b shows the power law relationship between J_{sc} and light intensity. It is known that a carrier imbalance or an interfacial barrier could lead to a space charge limited solar cell with $\alpha \sim 0.75$.[47–49] An α value close to 1 means a solar cell with no space charge effect.[47–49] The PVSC with TRUX-E-T HSLs does not appear to be space charge limited since the α is 0.99, indicating an efficient charge transfer in this solar cell. The natural logarithmic relationship between light intensity and V_{oc} has a slope of $1.56k_BT/q$, as shown in Fig. 6c, implying that Shockley–Read–Hall recombination is dominant in solar cells,[50–52] which is also consistent with the fact that the FF decreases when the light intensity increases from 1 to 100 mW cm^{-2} (Fig. 6d). Therefore, the high FF originates from the efficient charge transfer at the perovskite/HSL interface due to the appropriate HOMO level and high hole mobility of HSLs.

The estimated lab synthesis and purification cost of TRUX-E-T is about $38.9 g^{-1} (see the cost calculation for TRUX-E-T in the ESI†), which is one thirteenth of that of spiro-OMeTAD (about $500 g^{-1}).[53] Furthermore, the typical thickness of spiro-OMeTAD for efficient PVSCs is around 150 nm, while the thickness of TRUX-E-T HSLs used in our PVSCs is only about 50 nm. Therefore, the unit cost of TRUX-E-T used in PVSCs is roughly one fortieth of that of spiro-OMeTAD.[53] Therefore, our TRUX-E-T HSL offers an attractive potential for commercialization of the emerging PVSC technology.

4. Conclusions

We have synthesized and characterized TRUX-E-T, a new small molecule-based HSL material using a facile route.

This journal is © The Royal Society of Chemistry 2017

J. Mater. Chem. A, 2017, 5, 23319–23327 | **23325**

Characterizations reveal that TRUX-E-T is suitable as a HSL for PVSCs. We found that TRUX-E-T can be smoothly deposited on perovskite layers, enabling PVSCs to use thin TRUX-E-T layers. Our best-performing PVSCs use only ~50 nm thick TRUX-E-THSLs, which facilitates the reduction in device cost. The estimated unit cost of TRUX-E-T used in PVSCs is roughly one 40th of that of spiro-OMeTAD. Finally, TRUX-E-T exhibits hole mobilities as high as 2.47×10^{-4} cm^2 V^{-1} s^{-1}, which is responsible for the high FFs of up to 82% obtained in our PVSCs using thin TRUX-E-THSLs.

Conflicts of interest

There are no conflicts to declare.

Acknowledgements

References

1 Q. Dong, Y. Fang, Y. Shao, P. Mulligan, J. Qiu, L. Cao and J. Huang, *Science*, 2015, **347**, 967–970.

2 D. B. Mitzi, S. Wang, C. A. Feild, C. A. Chess and A. M. Guloy, *Science*, 1995, **267**, 1473–1476.

3 B. Saparov and D. B. Mitzi, *Chem. Rev.*, 2016, **116**, 4558–4596.

4 W.-J. Yin, T. Shi and Y. Yan, *Adv. Mater.*, 2014, **26**, 4653–4658.

5 S. D. Stranks, G. E. Eperon, G. Grancini, C. Menelaou, M. J. P. Alcocer, T. Leijtens, L. M. Herz, A. Petrozza and H. J. Snaith, *Science*, 2013, **342**, 341–344.

6 G. Xing, N. Mathews, S. Sun, S. S. Lim, Y. M. Lam, M. Grätzel, S. Mhaisalkar and T. C. Sum, *Science*, 2013, **342**, 344–347.

7 W. S. Yang, B.-W. Park, E. H. Jung, N. J. Jeon, Y. C. Kim, D. U. Lee, S. S. Shin, J. Seo, E. K. Kim, J. H. Noh and S. I. Seok, *Science*, 2017, **356**, 1376–1379.

8 M. Liu, M. B. Johnston and H. J. Snaith, *Nature*, 2013, **501**, 395–398.

9 H. Zhou, Q. Chen, G. Li, S. Luo, T.-b. Song, H.-S. Duan, Z. Hong, J. You, Y. Liu and Y. Yang, *Science*, 2014, **345**, 542–546.

10 A. Kojima, K. Teshima, Y. Shirai and T. Miyasaka, *J. Am. Chem. Soc.*, 2009, **131**, 6050–6051.

11 H.-S. Kim, C.-R. Lee, J.-H. Im, K.-B. Lee, T. Moehl, A. Marchioro, S.-J. Moon, R. Humphry-Baker, J.-H. Yum, J. E. Moser, M. Grätzel and N.-G. Park, *Sci. Rep.*, 2012, **2**, 591.

12 N. Ahn, D.-Y. Son, I.-H. Jang, S. M. Kang, M. Choi and N.-G. Park, *J. Am. Chem. Soc.*, 2015, **137**, 8696–8699.

13 W. Ke, G. Fang, Q. Liu, L. Xiong, P. Qin, H. Tao, J. Wang, H. Lei, B. Li, J. Wan, G. Yang and Y. Yan, *J. Am. Chem. Soc.*, 2015, **137**, 6730–6733.

14 D. Bi, C. Yi, J. Luo, J.-D. Décoppet, F. Zhang, S. M. Zakeeruddin, X. Li, A. Hagfeldt and M. Grätzel, *Nat. Energy*, 2016, **1**, 16142.

15 M. Yang, Z. Li, M. O. Reese, O. G. Reid, D. H. Kim, S. Siol, T. R. Klein, Y. Yan, J. J. Berry, M. F. A. M. van Hest and K. Zhu, *Nat. Energy*, 2017, **2**, 17038.

16 D. Zhao, Y. Yu, C. Wang, W. Liao, N. Shrestha, C. R. Grice, A. J. Cimaroli, L. Guan, R. J. Ellingson, K. Zhu, X. Zhao, R.-G. Xiong and Y. Yan, *Nat. Energy*, 2017, **2**, 17018.

17 Y. Shao, Y. Yuan and J. Huang, *Nat. Energy*, 2016, **1**, 15001.

18 D. Zhao, M. Sexton, H.-Y. Park, G. Baure, J. C. Nino and F. So, *Adv. Energy Mater.*, 2015, **5**, 1401855.

19 A. Krishna and A. C. Grimsdale, *J. Mater. Chem. A*, 2017, **5**, 16446–16466.

20 J. Burschka, A. Dualeh, F. Kessler, E. Baranoff, N.-L. Cevey-Ha, C. Yi, M. K. Nazeeruddin and M. Grätzel, *J. Am. Chem. Soc.*, 2011, **133**, 18042–18045.

21 L. Calió, S. Kazim, M. Grätzel and S. Ahmad, *Angew. Chem., Int. Ed.*, 2016, **55**, 14522–14545.

22 J.-P. Correa-Baena, A. Abate, M. Saliba, W. Tress, T. Jesper Jacobsson, M. Gratzel and A. Hagfeldt, *Energy Environ. Sci.*, 2017, **10**, 710–727.

23 W. Yan, S. Ye, Y. Li, W. Sun, H. Rao, Z. Liu, Z. Bian and C. Huang, *Adv. Energy Mater.*, 2016, **6**, 1600474.

24 X. Yin, Q. An, J. Yu, F. Guo, Y. Geng, L. Bian, Z. Xu, B. Zhou, L. Xie, F. Zhang and W. Tang, *Sci. Rep.*, 2016, **6**, 25355.

25 K. Rakstys, A. Abate, M. I. Dar, P. Gao, V. Jankauskas, G. Jacopin, E. Kamarauskas, S. Kazim, S. Ahmad, M. Grätzel and M. K. Nazeeruddin, *J. Am. Chem. Soc.*, 2015, **137**, 16172–16178.

26 K. Rakstys, S. Paek, P. Gao, P. Gratia, T. Marszalek, G. Grancini, K. T. Cho, K. Genevicius, V. Jankauskas, W. Pisula and M. K. Nazeeruddin, *J. Mater. Chem. A*, 2017, **5**, 7811–7815.

27 C. Huang, W. Fu, C.-Z. Li, Z. Zhang, W. Qiu, M. Shi, P. Heremans, A. K. Y. Jen and H. Chen, *J. Am. Chem. Soc.*, 2016, **138**, 2528–2531.

28 J.-L. Wang, Z.-M. Tang, Q. Xiao, Y. Ma and J. Pei, *Org. Lett.*, 2009, **11**, 863–866.

29 P.-Y. Su, L.-B. Huang, J.-M. Liu, Y.-F. Chen, L.-M. Xiao, D.-B. Kuang, M. Mayor and C.-Y. Su, *J. Mater. Chem. A*, 2017, **5**, 1913–1918.

30 P. Ganesan, K. Fu, P. Gao, I. Raabe, K. Schenk, R. Scopelliti, J. Luo, L. H. Wong, M. Gratzel and M. K. Nazeeruddin, *Energy Environ. Sci.*, 2015, **8**, 1986–1991.

31 H. Li, K. Fu, A. Hagfeldt, M. Grätzel, S. G. Mhaisalkar and A. C. Grimsdale, *Angew. Chem., Int. Ed.*, 2014, **53**, 4085–4088.

32 J. Wang, K. Liu, L. Ma and X. Zhan, *Chem. Rev.*, 2016, **116**, 14675–14725.

33 H. Chen, W. Fu, C. Huang, Z. Zhang, S. Li, F. Ding, M. Shi, C.-Z. Li, A. K. Y. Jen and H. Chen, *Adv. Energy Mater.*, 2017, 1700012, DOI: 10.1002/aenm.201700012.

34 Y. Yu, C. Wang, C. R. Grice, N. Shrestha, J. Chen, D. Zhao, W. Liao, A. J. Cimaroli, P. J. Roland, R. J. Ellingson and Y. Yan, *ChemSusChem*, 2016, **9**, 3288–3297.

35 M. L. Petrus, T. Bein, T. J. Dingemans and P. Docampo, *J. Mater. Chem. A*, 2015, **3**, 12159–12162.

36 W. Ke, C. Xiao, C. Wang, B. Saparov, H.-S. Duan, D. Zhao, Z. Xiao, P. Schulz, S. P. Harvey, W. Liao, W. Meng, Y. Yu, A. J. Cimaroli, C.-S. Jiang, K. Zhu, M. Al-Jassim, G. Fang, D. B. Mitzi and Y. Yan, *Adv. Mater.*, 2016, **28**, 5214–5221.

37 C. Wang, C. Xiao, Y. Yu, D. Zhao, R. A. Awni, C. R. Grice, K. Ghimire, D. Constantinou, W. Liao, A. J. Cimaroli, P. Liu, J. Chen, N. J. Podraza, C.-S. Jiang, M. M. Al-Jassim, X. Zhao and Y. Yan, *Adv. Energy Mater.*, 2017, **7**, 1700414.

38 C. Wang, D. Zhao, C. R. Grice, W. Liao, Y. Yu, A. Cimaroli, N. Shrestha, P. J. Roland, J. Chen, Z. Yu, P. Liu, N. Cheng, R. J. Ellingson, X. Zhao and Y. Yan, *J. Mater. Chem. A*, 2016, **4**, 12080–12087.

39 C. Wang, L. Guan, D. Zhao, Y. Yu, C. R. Grice, Z. Song, R. A. Awni, J. Chen, J. Wang, X. Zhao and Y. Yan, *ACS Energy Lett.*, 2017, 2118–2124, DOI: 10.1021/acsenergylett.7b00644.

40 C. Wang, D. Zhao, Y. Yu, N. Shrestha, C. R. Grice, W. Liao, A. J. Cimaroli, J. Chen, R. J. Ellingson, X. Zhao and Y. Yan, *Nano Energy*, 2017, **35**, 223–232.

41 X. Yin, L. Guan, J. Yu, D. Zhao, C. Wang, N. Shrestha, Y. Han, Q. An, J. Zhou, B. Zhou, Y. Yu, C. R. Grice, R. A. Awni, F. Zhang, J. Wang, R. J. Ellingson, Y. Yan and W. Tang, *Nano Energy*, 2017, **40**, 163–169.

42 Y. Yu, C. Wang, C. R. Grice, N. Shrestha, D. Zhao, W. Liao, L. Guan, R. A. Awni, W. Meng, A. J. Cimaroli, K. Zhu, R. J. Ellingson and Y. Yan, *ACS Energy Lett.*, 2017, 1177–1182, DOI: 10.1021/acsenergylett.7b00278.

43 Q. Feng, X. Jia, G. Zhou and Z.-S. Wang, *Chem. Commun.*, 2013, **49**, 7445–7447.

44 W. Liao, D. Zhao, Y. Yu, N. Shrestha, K. Ghimire, C. R. Grice, C. Wang, Y. Xiao, A. J. Cimaroli, R. J. Ellingson, N. J. Podraza, K. Zhu, R.-G. Xiong and Y. Yan, *J. Am. Chem. Soc.*, 2016, **138**, 12360–12363.

45 B. Chen, M. Yang, X. Zheng, C. Wu, W. Li, Y. Yan, J. Bisquert, G. Garcia-Belmonte, K. Zhu and S. Priya, *J. Phys. Chem. Lett.*, 2015, 4693–4700, DOI: 10.1021/acs.jpclett.5b02229.

46 Y. Shao, Z. Xiao, C. Bi, Y. Yuan and J. Huang, *Nat. Commun.*, 2014, **5**, 5784.

47 D. Bi, L. Yang, G. Boschloo, A. Hagfeldt and E. M. J. Johansson, *J. Phys. Chem. Lett.*, 2013, **4**, 1532–1536.

48 L. J. A. Koster, V. D. Mihailetchi, H. Xie and P. W. M. Blom, *Appl. Phys. Lett.*, 2005, **87**, 203502.

49 V. D. Mihailetchi, J. Wildeman and P. W. M. Blom, *Phys. Rev. Lett.*, 2005, **94**, 126602.

50 S. R. Cowan, W. L. Leong, N. Banerji, G. Dennler and A. J. Heeger, *Adv. Funct. Mater.*, 2011, **21**, 3083–3092.

51 R. N. Hall, *Phys. Rev.*, 1952, **87**, 387.

52 W. Shockley and W. T. Read, *Phys. Rev.*, 1952, **87**, 835–842.

53 M. Saliba, S. Orlandi, T. Matsui, S. Aghazada, M. Cavazzini, J.-P. Correa-Baena, P. Gao, R. Scopelliti, E. Mosconi, K.-H. Dahmen, F. De Angelis, A. Abate, A. Hagfeldt, G. Pozzi, M. Graetzel and M. K. Nazeeruddin, *Nat. Energy*, 2016, **1**, 15017.